

# Self-bound crystals of antiparallel dipolar mixtures

Maria Arazo,<sup>1,2</sup> Albert Gallemí,<sup>3</sup> Montserrat Guilleumas,<sup>1,2</sup> Ricardo Mayol,<sup>1,2</sup> and Luis Santos<sup>3</sup>

<sup>1</sup>*Departament de Física Quàntica i Astrofísica, Universitat de Barcelona, Martí i Franquès 1, 08028 Barcelona, Spain*

<sup>2</sup>*Institut de Ciències del Cosmos, Universitat de Barcelona, Martí i Franquès 1, 08028 Barcelona, Spain*

<sup>3</sup>*Institut für Theoretische Physik, Leibniz Universität Hannover, 30167 Hannover, Germany*

(Dated: March 6, 2023)

Recent experiments have created supersolids of dipolar quantum droplets. The resulting crystals lack, however, a genuine cohesive energy and are maintained by the presence of an external confinement, bearing a resemblance to the case of ion Coulomb crystals. We show that a mixture of two antiparallel dipolar condensates allows for the creation of potentially large, self-bound crystals which, resembling ionic crystals in solid-state physics, are maintained by the mutual dipolar attraction between the components, with no need of transversal confinement. This opens intriguing novel possibilities, including three-dimensionally self-bound droplet-ring structures, stripe/labyrinthic patterns, and self-bound crystals of droplets surrounded by an interstitial superfluid, resembling the case of superfluid Helium in porous media.

Solid-state crystals are held together by the interplay between different forms of attractive and repulsive interactions between their constituents [1]. This interplay results in a finite cohesive or binding energy, defined as the energy that must be added to the crystal to separate its components infinitely apart. In the presence of an external confinement, crystals may form even in the absence of genuine cohesion. A prominent example is provided by trapped ions, which form crystals due to the combination of repulsive Coulomb interactions and external confinement [2]. There is, however, no cohesive energy, and ion Coulomb crystals unravel in the absence of the trap.

This feature is shared by recently created crystals of quantum droplets in dipolar Bose-Einstein condensates [3, 4]. Self-bound droplets, elongated along the dipole direction, result from the quasi-cancellation of contact and dipolar interactions, and the stabilizing effect of quantum fluctuations [5–8]. In the presence of confinement along the dipole direction, energy is minimized by the creation of multiple droplets, which, in the presence of an external confinement perpendicular to the dipole orientation (transversal trap), arrange forming a crystal [9] that may present supersolid properties [10–17]. Similar to the case of ions in Coulomb crystals, droplets repel each other. There is hence no genuine cohesive energy of the droplet crystal (or of any other possible density pattern [18–21]). The transversal trap is crucial to keep it bound.

Recent experiments have created a mixture of two dipolar components [22–24]. These mixtures are expected to present rich physics due to the competition between intra- and inter-component contact and dipolar interactions, including immiscible droplets [25, 26], doping-induced droplet nucleation [24, 27], two-fluid supersolidity [27], and the formation of alternating-domain supersolids [28–30]. Interestingly, the dipoles of the two components may be antiparallel, and hence the inter- and intra-component interactions may have opposite sign [29] (Fig. 1(a)).

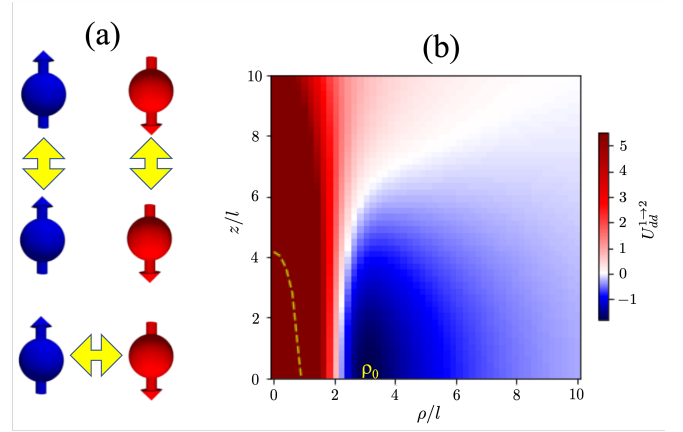


FIG. 1. (a) In an ADM, intra-component interactions are attractive (yellow arrows) when the particles are head-to-tail, and repulsive when they are side-by-side, whereas the opposite is true for the inter-component ones. (b) Dipolar interaction  $V_{\text{dd}}^{1 \rightarrow 2}(\mathbf{r}) = \frac{2\mu_0\mu_1^2}{3\pi l_z^2} U_{\text{dd}}^{1 \rightarrow 2}$  that component 1 exerts on component 2, as a function of  $z$  and  $\rho = \sqrt{x^2 + y^2}$ . For simplicity, we have assumed a Gaussian droplet  $e^{-z^2/l_z^2} e^{-\rho^2/2l^2}$ . The dashed line indicates the half-width-at-half-maximum of the droplet. The inter-component dipolar interaction results in an energy minimum on the  $xy$  plane at a given radius  $\rho_0$  well outside the droplet.

In this letter, we investigate crystal formation in an antiparallel dipolar mixture (ADM). As for a parallel one [25, 26], in the absence of any confinement, an ADM may form an immiscible three-dimensionally self-bound mixture, although with a markedly different topology in which one of the components may eventually form a ring around a droplet of the other. The presence of confinement along the dipole direction results in crystal formation. In stark contrast to both single-component dipolar condensates and parallel binary mixtures, in an ADM the crystal has a genuine cohesive energy, remaining self-bound in the absence of a transversal trap due

to the mutual attraction between the components. This resembles the case of ionic crystals in solid-state physics, where ions of opposite charge arrange in an intertwined crystalline structure bound by their mutual electrostatic interaction [1]. However, the resulting self-bound ADM is not given by two intertwined droplet arrays. Symmetric ADMs with similar intra-component interaction strengths form self-bound stripe/labyrinthic density patterns. In contrast, in sufficiently asymmetric ADMs, one of the components forms an incoherent droplet crystal with an approximate triangular structure, whereas the second one remains superfluid and fills the lattice interstitials, resembling to some extent superfluid Helium in porous media [31].

*Model.*— We consider a bosonic ADM, with dipoles oriented, respectively, along and antiparallel to the  $z$  axis. The components may belong to the same species or to two different ones. In order to illustrate the possible physics, we consider a dysprosium mixture, with magnetic dipoles  $\mu_1 = 10 \mu_B$  and  $\mu_2 = -10 \mu_B$ , with  $\mu_B$  the Bohr magneton. Short-range interactions are characterized by the intra- and inter-component scattering lengths:  $a_{11}$ ,  $a_{22}$ , and  $a_{12}$ . The physics of the mixture is well described by the extended Gross-Pitaevskii equation [25, 26]:

$$i\hbar\dot{\Psi}_\sigma(\mathbf{r}, t) = \left[ \frac{-\hbar^2\nabla^2}{2m} + V_{\text{trap}}(\mathbf{r}) + \sum_{\sigma'} g_{\sigma\sigma'} |\Psi_{\sigma'}(\mathbf{r}, t)|^2 + \sum_{\sigma'} \int d^3r' V_{\text{dd}}^{\sigma\sigma'}(\mathbf{r} - \mathbf{r}') |\Psi_{\sigma'}(\mathbf{r}', t)|^2 + \mu_{\text{LHY},\sigma}[n_{1,2}(\mathbf{r}, t)] \right] \Psi_\sigma(\mathbf{r}, t), \quad (1)$$

where  $\Psi_\sigma(\mathbf{r}, t)$  is the condensate wavefunction of component  $\sigma = 1, 2$ ,  $n_\sigma = |\Psi_\sigma|^2$ , and  $g_{\sigma\sigma'} = 4\pi\hbar^2 a_{\sigma\sigma'}/m$ , with  $m$  the mass of the bosons. The atoms are confined, if at all, only along the  $z$  axis by a potential  $V_{\text{trap}}(\mathbf{r}) = \frac{1}{2}m\omega_z^2 z^2$ . The dipole-dipole interaction is given by the potential  $V_{\text{dd}}^{\sigma\sigma'}(\mathbf{r}) = \frac{\mu_0\mu_\sigma\mu_{\sigma'}}{4\pi r^3} (1 - 3\cos^2\theta)$ , with  $\theta$  the angle sustained by the  $z$  axis and  $\mathbf{r}$ . The effect of quantum fluctuations is provided by the Lee-Huang-Yang (LHY) term  $\mu_{\text{LHY},\sigma}[n_{1,2}(\mathbf{r}, t)] = \delta E_{\text{LHY}}/\delta n_\sigma$ , where

$$E_{\text{LHY}} = \frac{8}{15\sqrt{2\pi}} \left( \frac{m}{4\pi\hbar^2} \right)^{3/2} \int d\theta_k \sin\theta_k \sum_{\lambda=\pm} V_\lambda(\theta_k)^{5/2} \quad (2)$$

is the LHY energy correction, with

$$V_\pm(\theta_k) = \sum_{\sigma=1,2} \eta_{\sigma\sigma} n_\sigma \pm \sqrt{(\eta_{11}n_1 - \eta_{22}n_2)^2 + 4\eta_{12}^2 n_1 n_2} \quad (3)$$

and  $\eta_{\sigma\sigma'} = g_{\sigma\sigma'} + g_{\sigma\sigma'}^d(3\cos^2\theta_k - 1)$ , being  $g_{\sigma\sigma'}^d = \mu_0\mu_\sigma\mu_{\sigma'}/3$  and  $\theta_k$  the angle sustained by  $\mathbf{k}$  with the  $z$  axis. Since the dipole moments of the components are antiparallel, the inter-component dipolar potential is repulsive (attractive) when the components are placed head-with-tail (side-by-side) (see Fig. 1(a)). As a result, the

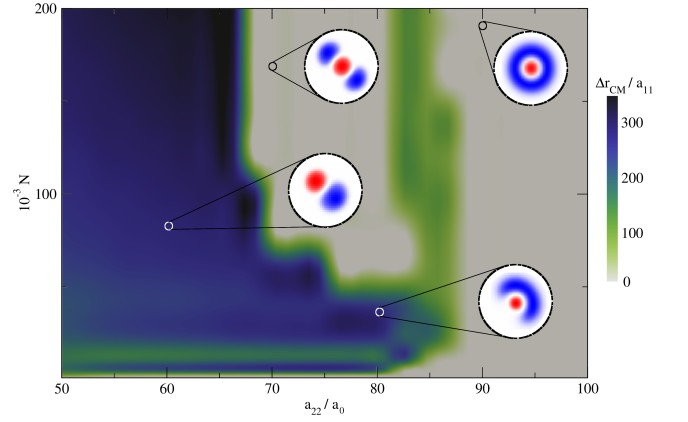


FIG. 2. Three-dimensionally self-bound ADMs. Ground-state configuration as a function of the total atom number  $N$  and of  $a_{22}$ , for  $a_{11} = 50 a_0$  and  $N_{1,2} = N/2$ . Whereas component 1 always forms a single elongated droplet, component 2 may acquire different topologies, which we characterize using the separation  $\Delta r_{\text{CM}}$  between the center of masses of the two components (color code). The different topologies are illustrated in the insets, where we depict the column density (integrated over  $z$ ) of the components, with red (blue) indicating component 1 (2).

dipolar interaction strongly favors immiscibility, and a very large and negative  $a_{12}$  is needed to drive the system miscible. In the following, we consider  $a_{12} = 150 a_0$ , but the actual value is irrelevant as long as the inter-component overlapping remains negligible.

*Three-dimensionally self-bound ADM.*— We first consider the case of fully unconfined mixtures ( $\omega_z = 0$ ). As for parallel dipolar mixtures [25, 26], an immiscible ADM may present a three-dimensionally self-bound solution, but of a markedly different nature. This is best understood in the impurity limit ( $N_1 \gg N_2$ ). Let us assume that component 1 forms a self-bound droplet with density  $n_1(\mathbf{r})$ . The droplet exerts a potential  $V_{\text{dd}}^{1\rightarrow 2}(\mathbf{r}) = \int d^3r' V_{\text{dd}}^{12}(\mathbf{r} - \mathbf{r}') n_1(\mathbf{r}')$  on component 2, which, as seen in Fig. 1(b), is characterized by a marked minimum at a given radius  $\rho_0$ , well outside the droplet. Particles in component 2 are trapped in this mexican-hat potential.

In a more balanced mixture, the argument remains valid, but component 2 also induces a similar potential  $V_{\text{dd}}^{2\rightarrow 1}(\mathbf{r})$  on component 1. Hence the two components confine each other mutually on the  $xy$  plane, resulting in self-bound ADMs, as illustrated in Fig. 2 for  $N_{1,2} = N/2$ ,  $a_{11} = 50 a_0$ , and different values of  $a_{22}$  and  $N$ . For asymmetric intra-component interactions  $a_{11} < a_{22}$ , component 1 remains a compact droplet, whereas the second component accommodates on the ring potential around the droplet. For low enough  $a_{22}$ , the energy is minimized by the formation of a single droplet in component 2, which for growing  $N$  and  $a_{22}$  spreads around the mexican-hat minimum until eventually forming a ring-like configuration. For intermediate  $a_{22}$  values, there is a

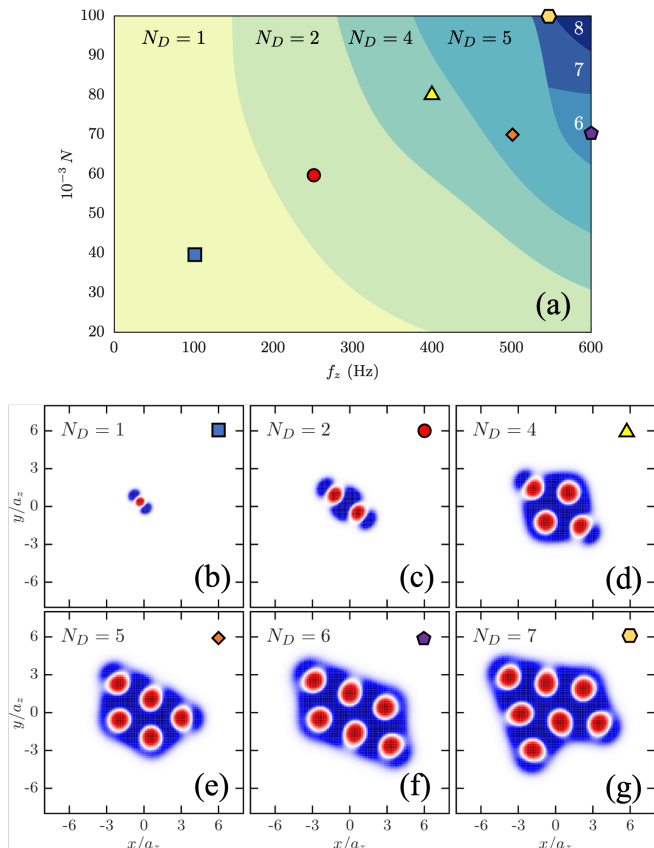


FIG. 3. Self-bound droplet crystals. (a) Phase diagram as a function of the atom number  $N$  and the trap frequency  $f_z = \omega_z/2\pi$ , for  $a_{11} = 50 a_0$  and  $a_{22} = 70 a_0$ . Colors correspond to configurations with a different number of droplets  $N_D$  in component 1. Figures (b–g) show the column magnetization (integrated along  $z$ ) of the lowest-energy solution for selected cases, indicated with the corresponding symbol in Fig. (a). Red (blue) regions are populated by component 1 (2).

second possible topology with two droplets of component 2 placed at opposite sides of the annular potential.

*Self-bound droplet crystals.*— When  $\omega_z = 0$ , increasing the particle number  $N$  results in more elongated solutions along the  $z$  direction. As for single-component (scalar) dipolar condensates [3], this elongation is frustrated in the presence of a trap along  $z$  ( $\omega_z > 0$ ). In scalar condensates, this frustration results in the formation of multiple droplets. Although the droplets repel each other, the presence of a transversal trap on the  $xy$  plane allows for the creation of 2D droplet crystals [16, 17]. These crystals have however no intrinsic cohesion, and hence unravel in the absence of the  $xy$  confinement.

Remarkably, this is not the case in an ADM, as illustrated in Fig. 3 for a balanced mixture  $N_1 = N_2$  and asymmetric intra-component interactions,  $a_{11} = 50 a_0$  and  $a_{22} = 70 a_0$ . For a low-enough  $\omega_z$ , the three-

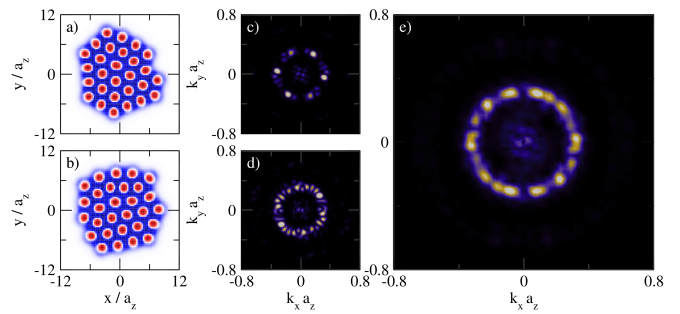


FIG. 4. (a,b) Single-shot realizations of the column magnetization for  $a_{11} = 50 a_0$ ,  $a_{22} = 70 a_0$ ,  $N_{1,2} = 5 \times 10^4$  and  $\omega_z/2\pi = 1300$  Hz. Red (blue) regions are populated by component 1 (2). (c,d) Corresponding momentum distribution for the second component,  $\tilde{n}_2(k_x, k_y)$  in the  $k_z = 0$  plane, in the cases of Figs. (a) and (b), respectively. (e) Momentum distribution  $\tilde{n}_2(k_x, k_y)$  averaged over 10 different realizations.

dimensional solution (with a single droplet in component 1) remains valid (Fig. 3(b)). For an  $N$ -dependent critical  $\omega_z$  the droplet splits into two. Each one of them exerts a mexican-hat potential on the second component, which gets trapped in the combined energy minimum. At the same time, crucially, the second component glues the two droplets together, forming a self-bound ADM (Fig. 3(c)). As shown in Fig. 3(a), and illustrated for particular cases in Figs. 3(d–g), further increasing  $\omega_z$  results in a growing number of droplets of component 1 surrounded by a bath of component 2. In a scalar condensate, each droplet requires a minimal atom number to remain self-bound (otherwise kinetic energy unbinds it), drastically limiting the total number of droplets. In contrast, in an ADM, droplets remain confined by the inter-component interaction, allowing for droplets with a much smaller number of atoms [28, 29]. As a result, increasing  $\omega_z$  results in 2D crystals with much more droplets compared to scalar condensates with the same total number of atoms.

We should emphasize that our results, based on imaginary-time evolution of Eq. (1) with random initial conditions, reveal many possible solutions with very similar energy, which differ in the exact number and arrangement of the droplets (see [32]). We hence expect a significant experimental shot-to-shot variability, similar to that recently observed in experiments on 2D supersolids [16].

*Interstitial superfluid.*— Due to the lack of overlapping, the droplets are mutually incoherent. In contrast, the component filling the crystal interstitials forms a superfluid that resembles, to some extent, the case of Helium in a porous medium (although, in contrast to that scenario, droplets of component 1 do not form a rigid structure). The approximately triangular crystalline structure of the droplets is inherited as well by the interstitial component 2, which builds hence a peculiar form of supersolid. The coherence and spatial density modulation of component 2 may be revealed in time-

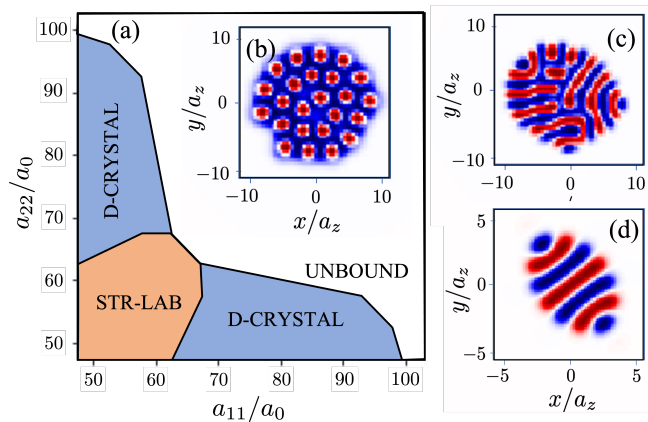


FIG. 5. (a) Phase diagram for  $N_{1,2} = 5 \times 10^4$  and  $\omega_z/2\pi = 1200$  Hz. Two different self-bound solutions are found: a droplet crystal (D-CRYSTAL), illustrated in Fig. (b) for  $a_{11} = 50 a_0$  and  $a_{22} = 70 a_0$ , and a stripe/labyrinthic (STR-LAB) phase, illustrated in Fig. (c) for  $a_{11} = 55 a_0$  and  $a_{22} = 60 a_0$ . The case of a well-defined stripe phase is illustrated in Fig. (d), which has been evaluated for  $\omega_z/2\pi = 180$  Hz,  $a_{11} = 80 a_0$ , and  $a_{22} = 80 a_0$ . In Figs. (b–d) we depict the column magnetization. Red (blue) regions are populated by component 1 (2).

of-flight measurements. Figure 4 shows the momentum distribution  $\tilde{n}_2(k_x, k_y)$  in the  $k_z = 0$  plane. The approximate triangular structure (Fig. 4(a)) results in an hexagonal pattern in the  $\tilde{n}_2$  distribution (Fig. 4(c)), although the above-mentioned variability of the exact droplet arrangement may result in a significant shot-dependent distortion (see Figs. 4(b,d)). Note as well that, due to the lack of any confinement on the  $xy$  plane, the patterns spontaneously break the polar symmetry and hence experience a random rotation from shot to shot. In any case, as expected from the theory of roton immiscibility [29, 33], the inter-droplet distance  $R$  is fixed by the oscillator length  $a_z = \sqrt{\hbar/m\omega_z}$ . For the case of Fig. 3,  $R \simeq 3 a_z$  for all values of  $N$  and  $\omega_z$ . This periodicity becomes evident from the average of the momentum distribution over many realizations, which shows a marked ring at  $1/R$  (see Fig. 4(e)).

*Crystal sublimation.*— For a fixed total number of particles, the cohesive energy decreases when the droplet number grows, since lowering the density reduces the inter-component dipolar attraction. Eventually, at a critical frequency  $\omega_z^{\text{cr}}$ , the crystal unbinds, and both components evaporate. The critical frequency ( $\omega_z^{\text{cr}}/2\pi \simeq 1400$  Hz for the case on Fig. 3) is approximately determined as that for which the energy per particle reaches  $\hbar\omega_z/2$ , corresponding to an infinitely spread solution on the  $xy$  plane. Interestingly, when  $\omega_z$  approaches  $\omega_z^{\text{cr}}$ , mutual attraction may still be enough to maintain a stable crystal, but insufficient to bind the whole interstitial superfluid, which hence partially evaporates (see [32] for a more detailed discussion).

*Self-bound stripe/labyrinthic patterns.*— Up to this point, we have considered a mixture with markedly asymmetric intra-component interactions. Interestingly, when  $a_{11} \simeq a_{22}$ , the mixture arranges in a different form of self-bound pattern (note that  $a_{11} = a_{22}$  if we consider a mixture of two maximally stretched magnetic states of the same atomic species). This is illustrated by the phase diagram of Fig. 5 (a), obtained for  $\omega_z/2\pi = 1200$  Hz and  $N_{1,2} = 5 \times 10^4$ . For sufficiently large  $|a_{11} - a_{22}|$ , we obtain the above-mentioned droplet crystal (Fig. 5(b)), which, as mentioned above, presents partial evaporation of the interstitial component in the vicinity of the unbinding threshold. In contrast, when  $a_{11} \simeq a_{22}$  the mixture arranges in a labyrinthic phase, with a large shot-to-shot variability, formed by stripes with different orientations (Fig. 5(c)). For lower trap frequencies, the ground-state configuration is given by a well-defined stripe crystal (Fig. 5(d)). Note that in the labyrinthic/stripe phase both components form mutually incoherent domains.

*Summary and Outlook.*— Antiparallel dipolar mixtures allow for the formation of crystals with a genuine cohesive energy that remain self-bound in the absence of a transversal trap. The mutual confinement stems from the attractive inter-component interactions, and results in incoherent stripe/labyrinthic crystals in mixtures with symmetric intra-component interactions, and self-bound droplet crystals in asymmetric mixtures. The latter are particularly interesting, since while one component forms an approximately triangular array of incoherent droplets, the other component builds a superfluid in the interstitials, forming a peculiar form of supersolid that may be readily probed using time-of-flight measurements. Although we have considered the particular example of a dysprosium mixture, our results generally apply to other antiparallel magnetic or electric dipolar mixtures, including those of polar molecules.

The possibility of creating self-bound dipolar crystals opens intriguing perspectives for future studies, including the character of lattice excitations, which may remain self-bound or result in phonon evaporation (resembling droplet evaporation in non-dipolar mixtures [5]), the probing (e.g. by vortex formation) of the superfluidity of the interstitial component, as well as in general the exploration of the dynamics of self-bound crystals.

This work has been supported by Grant No. PID2020-114626GB-I00 (Ministerio de Ciencia e Innovación), by the European Union Regional Development Fund within the ERDF Operational Program of Catalunya (project QUASICAT/QuantumCat), by the Deutsche Forschungsgemeinschaft (DFG, German Research Foundation) under Germany's Excellence Strategy—EXC-2123 QuantumFrontiers—390837967, and FOR 2247. M. A. is supported by FPI Grant PRE2018-084091.



- 
- [1] C. Kittel, [Introduction to Solid State Physics](#), 8th ed. (Wiley, 2004).
- [2] R. C. Thompson, [Contemporary Physics](#) **56**, 63 (2015), <https://doi.org/10.1080/00107514.2014.989715>.
- [3] F. Böttcher, J.-N. Schmidt, J. Hertkorn, K. S. H. Ng, S. D. Graham, M. Guo, T. Langen, and T. Pfau, [Reports on Progress in Physics](#) **84**, 012403 (2020).
- [4] L. Chomaz, I. Ferrier-Barbut, F. Ferlaino, B. Laburthe-Tolra, B. L. Lev, and T. Pfau, [Reports on Progress in Physics](#) **86**, 026401 (2022).
- [5] D. S. Petrov, [Phys. Rev. Lett.](#) **115**, 155302 (2015).
- [6] H. Kadau, M. Schmitt, M. Wenzel, C. Wink, T. Maier, I. Ferrier-Barbut, and T. Pfau, [Nature](#) **530**, 194 (2016).
- [7] L. Chomaz, S. Baier, D. Petter, M. J. Mark, F. Wächtler, L. Santos, and F. Ferlaino, [Phys. Rev. X](#) **6**, 041039 (2016).
- [8] M. Schmitt, M. Wenzel, F. Böttcher, I. Ferrier-Barbut, and T. Pfau, [Nature](#) **539**, 259 (2016).
- [9] M. Wenzel, F. Böttcher, T. Langen, I. Ferrier-Barbut, and T. Pfau, [Phys. Rev. A](#) **96**, 053630 (2017).
- [10] L. Tanzi, E. Lucioni, F. Famà, J. Catani, A. Fioretti, C. Gabbanini, R. N. Bisset, L. Santos, and G. Modugno, [Phys. Rev. Lett.](#) **122**, 130405 (2019).
- [11] F. Böttcher, J.-N. Schmidt, M. Wenzel, J. Hertkorn, M. Guo, T. Langen, and T. Pfau, [Phys. Rev. X](#) **9**, 011051 (2019).
- [12] L. Chomaz, D. Petter, P. Ilzhöfer, G. Natale, A. Trautmann, C. Politi, G. Durastante, R. M. W. van Bijnen, A. Patscheider, M. Sohmen, M. J. Mark, and F. Ferlaino, [Phys. Rev. X](#) **9**, 021012 (2019).
- [13] G. Natale, R. M. W. van Bijnen, A. Patscheider, D. Petter, M. J. Mark, L. Chomaz, and F. Ferlaino, [Phys. Rev. Lett.](#) **123**, 050402 (2019).
- [14] L. Tanzi, S. M. Roccuzzo, E. Lucioni, F. Famà, A. Fioretti, C. Gabbanini, G. Modugno, A. Recati, and S. Stringari, [Nature](#) **574**, 382 (2019).
- [15] M. Guo, F. Böttcher, J. Hertkorn, J.-N. Schmidt, M. Wenzel, H. P. Büchler, T. Langen, and T. Pfau, [Nature](#) **574**, 386 (2019).
- [16] M. A. Norcia, C. Politi, L. Klaus, E. Poli, M. Sohmen, M. J. Mark, R. N. Bisset, L. Santos, and F. Ferlaino, [Nature](#) **596**, 357 (2021).
- [17] T. Bland, E. Poli, C. Politi, L. Klaus, M. A. Norcia, F. Ferlaino, L. Santos, and R. N. Bisset, [Phys. Rev. Lett.](#) **128**, 195302 (2022).
- [18] Y.-C. Zhang, F. Maucher, and T. Pohl, [Phys. Rev. Lett.](#) **123**, 015301 (2019).
- [19] Y.-C. Zhang, T. Pohl, and F. Maucher, [Phys. Rev. A](#) **104**, 013310 (2021).
- [20] J. Hertkorn, J.-N. Schmidt, M. Guo, F. Böttcher, K. S. H. Ng, S. D. Graham, P. Uerlings, T. Langen, M. Zwierlein, and T. Pfau, [Phys. Rev. Res.](#) **3**, 033125 (2021).
- [21] E. Poli, T. Bland, C. Politi, L. Klaus, M. A. Norcia, F. Ferlaino, R. N. Bisset, and L. Santos, [Phys. Rev. A](#) **104**, 063307 (2021).
- [22] A. Trautmann, P. Ilzhöfer, G. Durastante, C. Politi, M. Sohmen, M. J. Mark, and F. Ferlaino, [Phys. Rev. Lett.](#) **121**, 213601 (2018).
- [23] G. Durastante, C. Politi, M. Sohmen, P. Ilzhöfer, M. J. Mark, M. A. Norcia, and F. Ferlaino, [Phys. Rev. A](#) **102**, 033330 (2020).
- [24] C. Politi, A. Trautmann, P. Ilzhöfer, G. Durastante, M. J. Mark, M. Modugno, and F. Ferlaino, [Phys. Rev. A](#) **105**, 023304 (2022).
- [25] J. C. Smith, D. Baillie, and P. B. Blakie, [Phys. Rev. Lett.](#) **126**, 025302 (2021).
- [26] R. N. Bisset, L. A. P. n. Ardila, and L. Santos, [Phys. Rev. Lett.](#) **126**, 025301 (2021).
- [27] D. Scheiermann, L. A. P. n. Ardila, T. Bland, R. N. Bisset, and L. Santos, [Phys. Rev. A](#) **107**, L021302 (2023).
- [28] S. Li, U. N. Le, and H. Saito, [Phys. Rev. A](#) **105**, L061302 (2022).
- [29] T. Bland, E. Poli, L. A. P. n. Ardila, L. Santos, F. Ferlaino, and R. N. Bisset, [Phys. Rev. A](#) **106**, 053322 (2022).
- [30] W. Kirkby, T. Bland, F. Ferlaino, and R. N. Bisset, (2023), [10.48550/ARXIV.2301.08007](https://arxiv.org/abs/10.48550/ARXIV.2301.08007).
- [31] J. D. Reppy, [Journal of Low Temperature Physics](#) **87**, 205 (1992).
- [32] See Supplemental Material at [URL will be inserted by publisher] for additional details on XXX.
- [33] R. M. Wilson, C. Ticknor, J. L. Bohn, and E. Timmermans, [Phys. Rev. A](#) **86**, 033606 (2012).

## Supplementary Information

The supplementary information contains additional details on the variability of the density patterns and the partial evaporation of the mixture mentioned in the main text.

### Shot-to-shot variability

There is a large shot-to-shot variability of the exact number of droplets and their arrangement in the droplet crystal. We illustrate this point with Fig. S1, where we show different configurations for the same parameters  $a_{11} = 50 a_0$ ,  $a_{22} = 70 a_0$ ,  $\omega_z/2\pi = 1200$  Hz, and  $N_{1,2} = 5 \times 10^4$ . The configurations, which have an energy per particle  $E/N \simeq 0.22 \hbar\omega_z$ , differ in energy by less than 1%, and have a number of droplets ranging from 23 to 31.

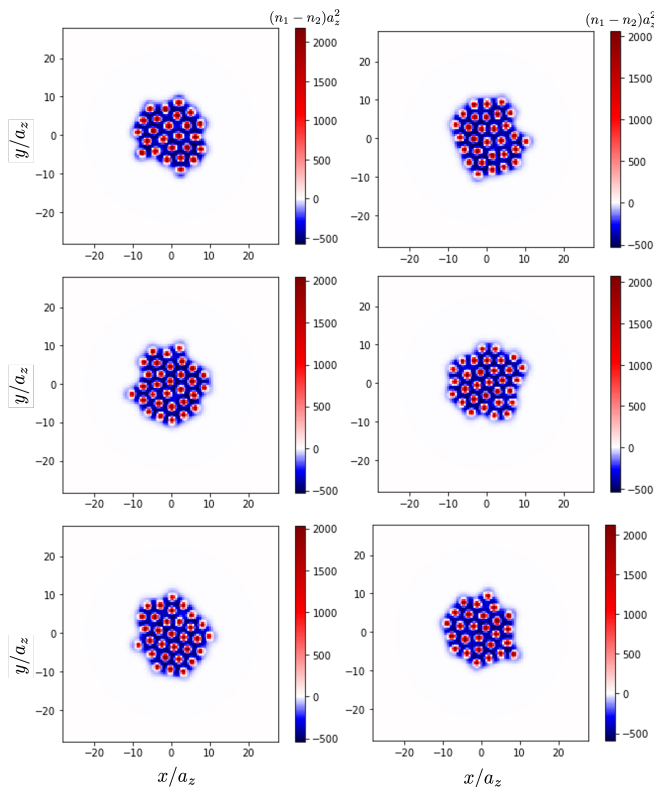


FIG. S1. Shot-to-shot variability. Different droplet lattice configurations obtained for the same parameters  $a_{11} = 50 a_0$ ,  $a_{22} = 70 a_0$ ,  $\omega_z/2\pi = 1200$  Hz,  $N_{1,2} = 5 \times 10^4$ . The plots show the column magnetization, with red (blue) indicating component 1 (2).

Note that the droplet arrangement is only approximately triangular, and the actual distribution, which is

generally non-uniform, may significantly depart from a triangular lattice. This is reflected in the structure of the interstitial component, which results in the distorted momentum distributions depicted in Fig. 4 of the main text. A similar shot-to-shot variability is observed in the stripe/labyrinthic phase.

### Evaporation of the droplet crystal

When  $\omega_z$  increases, the number of droplets grows and the density decreases. As a result, the cohesive energy is reduced, and the self-bound solution eventually unbinds. Figure S2 shows the energy per particle as a function of the trap frequency for  $a_{11} = 50 a_0$ ,  $a_{22} = 70 a_0$  and  $N_{1,2} = 5 \times 10^4$ . The unbinding of the droplet crystal occurs approximately when the energy per particle  $E/N$  reaches  $\hbar\omega_z/2$ , which, for the case of Fig. S2, occurs at  $\omega_z^{\text{cr}}/2\pi \simeq 1400$  Hz. Indeed, beyond that value we do not find well defined self-bound solutions in our simulations.

When  $\omega_z$  approaches  $\omega_z^{\text{cr}}$ , the crystal remains bound, but the interstitial component may present partial evaporation. In order to take this into account we considered absorbing boundary conditions in our imaginary-time simulations. We fixed a given radius  $\rho_c$  on the  $xy$  plane, such that the crystal is well contained in a circle of radius  $\rho < \rho_c$ . Particles that reach  $\rho > \rho_c$  during imaginary-time evolution are considered as evaporated. We indicate in Fig. S2 the proportion of the interstitial component that is evaporated, which as expected grows when approaching  $\omega_z^{\text{cr}}$ . In the unbound regime, the whole mixture eventually leaves (in imaginary time) the region  $\rho < \rho_c$ .

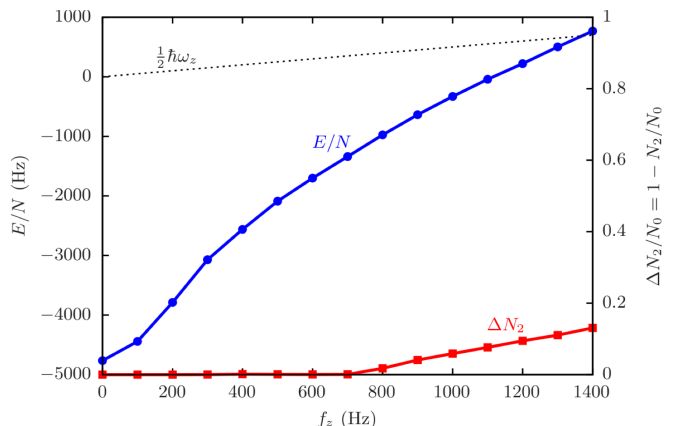


FIG. S2. Energy per particle (blue circles) as a function of the trap frequency for  $a_{11} = 50 a_0$ ,  $a_{22} = 70 a_0$  and  $N_{1,2} = 5 \times 10^4$ . The dashed line depicts the energy per particle ( $\hbar\omega_z/2$ ) corresponding to an infinitely spread mixture on the  $xy$  plane. The red squares indicate the proportion of atoms in component 2 which are evaporated (see text).